CERN/SPSC/85-20
SPSC/P 211
11 March 1985

P R O P O S A L

STUDY OF HIGH-ENERGY NUCLEUS-NUCLEUS INTERACTIONS WITH THE ENLARGED NA10 DIMUON SPECTROMETER

Bergen[1]-Bordeaux[2]-CERN[3]-Clermont-Ferrand[4]-
Ecole Polytechnique[5]-Lisbon[6]-Lyon[7]-Neuchâtel[8]-Orsay[9]-
Strasbourg[10]-Valencia[11] Collaboration

A. Baldit[4], G.P. Barreira[6], M. Bedjidian[7], P. Bordalo[6],
S. Borenstein[5], J. Britz[10], P. Busson[5], A. Casaca[6],
J. Castor[4], B. Chaurand[5], E. Descroix[7], J. Fargeix[4],
P. Force[4], J.M. Gago[6], C. Gerschel[9], P. Gorodetzky[10],
A. Guichard[7], R. Haroutunian[7], P.S. Iversen[1*], L. Kluberg[5],
G. Landaud[4], A. Maio[6], D. Perrin[8], G. Peyrard[4],
M. Pimenta[6], J.R. Pizzi[7], J. Quebert[2], S. Ramos[6],
A. Romana[5], R. Salmeron[5], P. Sonderegger[3],
J. Varela[6], and J. Velasco[11**]

1 Dept. of Physics, University of Bergen, Norway.
2 Centre d'Etudes Nucléaires, Univ. de Bordeaux I, Gradignan, France.
3 CERN, Geneva, Switzerland.
4 Lab. de Physique Corpusculaire, Université de Clermont-Ferrand, France.
5 LPNHE, Ecole Polytechnique, Palaiseau, France.
6 INIC, Instituto Nacional de Investigaçao Cientifica, Lisbon, Portugal.
7 Inst. de Physique Nucléaire, Université de Lyon, Villeurbanne, France.
8 Inst. de Physique, Université de Neuchâtel, Neuchâtel, Switzerland.
9 Inst. de Physique Nucléaire, Université de Paris-Sud, Orsay, France.
10 Centre de Recherches Nucléaires and Université Louis Pasteur, Strasbourg, France.
11 Facultad de Ciencias (IFIC), Burjasot, Valencia, Spain.
* At present Fellow at CERN, Geneva, Switzerland.
** Subject to approval by the Spanish High-Energy Physics Commission.

0001C/SB/sm

ABSTRACT

We propose to study dimuon production in ^{16}O-^{238}U collisions at the maximum expected luminosity (2×10^7 interactions per pulse), using the NA10 spectrometer to which we add beam counters, an active segmented target and an electromagnetic calorimeter. Thermal dimuons are expected to be emitted from a quark-gluon plasma at a reasonable rate in the 1-3 GeV/c^2 transverse mass range, and to differ from ordinary dimuons by their p_T and rapidity distribution. The correlations of the dimuon variables with charged multiplicity and neutral energy flow distributions will be studied event by event. The energy density is estimated directly from the transverse neutral energy. Prior to the oxygen runs, p-^{238}U collisions will be studied in the same apparatus with the twofold purpose of optimizing the layout and of establishing a data base suitable for extrapolation to ^{16}O-^{238}U collisions, deviations from which will then signal collective effects.

A fraction of the data will be taken with lighter targets, in order to extend the Drell-Yan systematics to nucleus-nucleus reactions. The apparatus is able to make full use of any admixture of heavier ions in the beam (^{40}Ca).

1. INTRODUCTION

In 1986, it will become possible to accelerate ^{16}O ions in the SPS to 225 GeV/nucleon (3.6 TeV/ion). The total energy pumped into small reaction volumes in, say, central O-U interactions will lead to energy densities several times higher than those which could previously be achieved in accelerator or collider experiments. Not more than a few dozen cosmic ray events have so far explored this domain, and found it promising indeed.

The interest in ultrarelativistic nucleus-nucleus physics has been considerably boosted by recent theoretical speculations which expect that, at very high temperature and/or energy density, matter will exist in a new phase, as a plasma of quarks and gluons ("QUAGMA"). Such speculations do not exclude that such a state might be produced when SPS ion beams hit heavy targets. At very high-energy densities the produced quarks would thermalize, i.e. interact among themselves many times before they hadronize.

The cleanest way to study the densities and momentum distributions of interacting quarks and antiquarks is offered by the emission of virtual photons. One extreme case is the Drell-Yan dileptons which probe the quarks of the highest relative energy: those which form the colliding nucleons. On the other extreme the low-energy secondary quarks and antiquarks will hardly produce dileptons except if the plasma exists, at temperatures not below ~ 200 MeV, in which case they are forced to interact very many times. Recent theoretical work suggests that the transverse mass of the thermal dileptons will then peak not at 200 MeV but above 1 GeV. Dimuons become therefore a suitable tool. Rate estimates are encouraging.

We propose to study dimuon production in ^{16}O nucleus interactions in the 1-5 GeV/c^2 mass range, at the highest available beam energy and intensity. We propose to use the NA10 multimuon spectrometer and to exploit its good acceptance for the low-energy dimuons for the central region of the nucleon-nucleon system where the Drell-Yan pairs peak and where the thermal dimuons are expected. The envisaged layout in shown in Fig. 1.

We propose to add to the NA10 spectrometer beam counters, an active target and an electromagnetic calorimeter. The purposes of these combined detectors are:

- to identify the incoming ion;

- to identify a central interaction inside a target where 20% of the beam will interact;

- to measure the energy density ϵ (through the total transverse neutral energy at $y_{c.m.} = 0$), which is the basic variable which is thought to govern the emergence of a plasma state.

These detectors explore further aspects which shed light on the reaction mechanisms:

- pseudorapidity and azimuthal distribution of charged particles;

- pseudorapidity and azimuthal distribution of neutral energy;

- production of direct bremsstrahlung photons.

We intend to trigger on dimuons, and to study all relevant correlations off-line. The proposed detector system will be able to handle a beam rate of 10^8 ions/2 s.

The proposed layout leaves some space suitable for a study of strangeness production in the target fragmentation region, where an enhanced K/π ratio would be a meaningful signal. Such an extension is beyond the reach of our collaboration in its present state.

In Section 2, we will discuss the physics motivations and goals of this experiment. Section 3 describes the NA10 spectrometer optimized for low-mass, low-rapidity dimuons. Section 4 describes the new equipment proposed for the target region. Section 5 discusses improvements and changes of the data acquistion system. Section 6 contains our beam requests.

2. PHYSICS MOTIVATIONS AND GOALS

In this section, we will deal with the issues of quagma formation, of dilepton emission by quagma and via other mechanisms, and of direct photon emission, all as seen in the context of the proposed experiment.

2.1 Quagma formation versus energy density

The bag model and more recently QCD lattice calculations [BIE 82, BNL 83, HEL 84] predict that deconfinement of quarks and gluons should occur if the density of hadrons becomes large compared to that of hadrons in ordinary nuclear matter. As a consequence, a new state of matter would be formed, a plasma of quarks and gluons (quagma). There is a degree of consensus that the transition should take place at a temperature T_c close to the Hagedorn temperature, $T_c \simeq 200 \pm 50$ MeV; but the needed energy density and the type of transition are much more uncertain. Indeed, the "experimental methods" in QCD calculations, which are being improved, may well one day exclude the quagma idea altogether, or make the transition indetectably smooth, or place it beyond the regions accessible to us. After this remark of caution, we turn to a more optimistic point of view.

Recent UA1 [ARN 82] and JACEE [BUR 84] data are not incompatible with an interpretation in terms of a first-order phase transition [GYU 84]. "Melting" of hadrons into quagma would set in at some energy density ε_H but would be complete only at a much higher density ε_Q. Temperature and pressure would be constant through the mixed phase transition region ($\varepsilon_H \leq \varepsilon \leq \varepsilon_Q$) and would result in a constant $\langle p_T \rangle$. The few JACEE events obtained at the very highest energy densities point at a dramatic increase in $\langle p_T \rangle$ setting in above ε_Q.

One widely used estimate for the energy density achieved in the central region of nucleon and nucleus high-energy reactions is [BJO 83]

$$\varepsilon = \frac{3}{2} \frac{dN_{ch}/dy|_{y=o} \times \langle M_T \rangle}{\pi \times R^2 \times ct_o} \ (\mathrm{GeV/fm^3}) \qquad (1)$$

where dN_{ch}/dy is the charged particle rapidity distribution, $M_T = \sqrt{M^2 + p_T^2}$, R is the transverse radius of the reaction volume, and t_o is the quark formation time. One chooses often [e.g.

BUR 84] t_o = 1 fm/c, which is somewhat arbitrary, and R = $A_{min}^{1/3}$ fm, where A_{min} is the atomic number of the smaller involved nucleus. One also uses dN/dη for dN/dy. With this scale, and using measured values for dN/dη and $\langle M_T \rangle$, the highly hypothetical transition region of the above picture extends from $\varepsilon_H \simeq$ 0.5 GeV/fm^3 to $\varepsilon_Q \simeq$ 3 GeV/fm^3.

On the same scale and using $\langle M_T \rangle$ = 0.4 GeV and reasonable assumptions for dN/dη [GAR 85 and Appendix A], we find ε_O = 2 and ε_{Ca} = 2.6 GeV/fm^3 for ^{16}O and ^{40}Ca central collisions with ^{238}U nuclei at 225 GeV/nucleon. Most of the 1986/87 SPS experimentation would take place, in the above picture, in the mixed phase region, where $\langle p_T \rangle$ would stay constant, but thermal photon and dilepton emission would gradually build up. On the other hand, fluctuations might give rise to a few events at $\varepsilon > \varepsilon_Q$.

[We use the usual rapidity and pseudorapidity variables $y = \ln (E + p_{//})/M_T$ and $\eta = \ln (p + p_{//})/p_T = -\ln \text{tg } \theta/2$, with three units difference between their values in the laboratory and the centre of mass.]

2.2 Measurement of energy density

The most direct measurement of ε which we propose in this experiment uses the transverse neutral energy flow $dE_T^o/d\eta$ as measured by the electromagnetic calorimeter (Section 4.2), according to a modified form of Eq. (1):

$$\varepsilon = 3 \frac{dE_T^o/d\eta|_{\eta=o}}{\pi \times R^2 \times ct_o} . \qquad (2)$$

At the same time, we will measure $dN_{ch}/d\eta$ and thereby, equating (1) and (2), get an estimate of $\langle M_T \rangle$, the average transverse energy of the produced hadrons, with $\langle M_T \rangle \simeq \langle p_T \rangle$. The interest of performing both measurements independently is illustrated by some of the highest ε JACEE events, where high values of $\langle p_T \rangle$ have been found in conjunction with a remarkable drop in charged multiplicity N_{ch} and dN/dη [BUR 84].

2.3 Emission and detection of dileptons from Quagma

The general features of real and virtual photon emission from a plasma of quarks and gluons have been computed [SHU 80, KAJ 82, MCL 85, HWA 85]. The basic analogy with, for example, emission of Drell-Yan pairs is complicated by the fact that the temperature which governs the quark density and spectrum in a plasma is difficult to predict and that it decreases with time while the plasma expands and cools. The recent calculations (MCL 85, HWA 85] take into account the hydrodynamic equations. The main consequences which are of interest for this experiment are:

- Importance, in the integration over the history of a plasma event, of dileptons emitted at high temperature, soon after the quark formation time τ_o. The smaller τ_o, the higher the dominating temperature. The parameter τ_o has played a rather formal rôle in setting the ϵ scale in equations (1) and (2). Here, its uncertain definition and possible A dependence is crucial in that it causes a much larger uncertainty in the integrated emission of dileptons. The rate predictions range from somewhat below the Drell-Yan rate to 2-3 orders of magnitude above it [MCL 85].

- Hydrodynamics play an important rôle in the relevant integrals and lead to transverse dilepton masses of [MCL 85, HWA 85]

$$M_T \simeq (2/v_s^2 + 1/2)T \geq 6.5\ T \qquad (3)$$

where $v_s \leq \sqrt{1/3}$ is the sound velocity in the plasma. This is much higher than the usual relation $\langle M_T \rangle \simeq 2\ T_c$ found, for example, for final state hadron emission (T_c is then the hadronization temperature, $T > T_c$). If quagma is produced at the SPS, its dilepton spectrum should peak between one and several GeV/c^2.

- Since the thermal dilepton rate is found to depend on the dilepton mass M and its transverse momentum p_T through the variable M_T only, the remarkable relationship $\langle p_T^2 \rangle = M^2$ is predicted.

- The rapidity distribution of thermal dimuons will reflect the plasma distribution, and peak at somewhat smaller rapidities than Drell-Yan pairs, in O-U collisions.

A possible experimental procedure to identify quagma dimuons may consist in sorting out samples of high p_T, $\eta < 3$ dimuons and studying their relative frequency as a function of charged multiplicity or of transverse neutral energy, of target atomic number, and of beam energy.

2.4 The broader category of collective effects

Even if no quagma is formed, the experiment remains quite ideally suited for the search for collective effects in a broader sense. The Drell-Yan pairs above the ψ have been shown to be produced proportionally to A^{α}, with $\alpha \simeq 1 \pm 0.03$ in proton-nucleus collisions [ITO 84]. The very low interaction probability of c quarks leads to an almost identical situation for the rather copious ψ production. These cross-sections should also scale linearly with the projectile mass.

In this experiment we intend to perform a careful comparison of dimuon and ψ production in proton-nucleus and in nucleus-nucleus interactions, with the same detector and set of targets, and at the same nucleon-nucleon c.m. energy. Any departure from $\beta = \alpha$ in the double parametrization $\sigma \sim A^{\beta}_{beam} \times A^{\alpha}_{target}$ would be an indication of collective effects.

2.5 Drell-Yan pairs in nucleus-nucleus collisions

We will similarly extend to nucleus-nucleus reactions the Drell-Yan systematics, by direct comparison of copious ^{16}O-^{238}U data beyond the ψ (and some data taken on lighter targets) with proton data taken with the same apparatus.

2.6 Emission and detection of direct photons

Quagma should radiate direct photons in amounts which are not negligible when compared to the π^o's. We will attempt to measure and understand the total neutral energy which accompanies a) dimuons in kinematic domains typical of Drell-Yan and hadronic production and b) dimuons compatible with thermal characteristics.

We intend also to concentrate on the special case of bremsstrahlung photons, which have been recently identified in K^+p collisions at 70 GeV/c (one photon of $E_{c.m.}$ = 20-60 MeV emitted every four events, at

very small angles $\theta_{lab} \lesssim 10$ mrad) [CHL 84, GOL 85]. We plan to extend the measurement of the electromagnetic energy flow into the very forward region, 2-10 mrad, where the photons from this process may compete with the very few expected high-energy π^o's.

3. THE DIMUON DETECTOR

The proposed apparatus is based on the NA10 multimuon spectrometer which will provide the muon pair signal used as trigger. The spectrometer and its characteristics, adapted for this specific experiment, are described hereafter.

3.1 Description of the current NA10 spectrometer

Figure 1 of Ref. [AND 84] shows a layout of the spectrometer as it is currently operating. It can detect any number of muons produced in an interaction in the target. Beam which does not interact is dumped into a tungsten and uranium plug 120 cm downstream of the target centre. This distance is large compared to the vertex resolution along the axis (21 cm) and thus the data are not contaminated by events from the beam dump. A carbon-iron absorber of 13.4 pion absorption lengths maintains multiple scattering and momentum resolution within bearable limits. It surrounds the beam dump plug and starts 40 cm downstream of the target centre, a distance which is small enough to reduce to a negligible level the fraction of high mass pairs of muons originating from pions or kaons which decay in flight between the target and the absorber. The 480 cm length of this muon filter can be adapted to less severe experimental conditions due to its 40 cm modularity. The spectrometer magnet is an air-core toroid with hexagonal symmetry which determines the geometrical structure of the scintillation counter hodoscopes R and the multiwire proportional chambers CP located upstream and downstream of the magnet. If good momentum resolution is required, then muons traversing only the air sectors of the magnet are selected. The fine granularity of the four hodoscopes (R1 to R4) used for the trigger allows a fast selection based on the transverse momentum of the muons. The individual coincidences between the very narrow counters of R1 and R2 are equivalent to a set of 32 telescopes per sextant which point to the target. At the trigger level, the muon candidates are detected by means of a quadruple coincidence between two counters of hodoscopes R1 and R2 and two counters of hodoscopes R3 and R4. The trigger requires a coincidence of two muon candidates in two

different sextants. Eight large proportional chambers measure the muon tracks. They are made of three planes each, with 2 mm spaced wires along three directions at 120 degrees. They are able to stand very high incident fluxes. The distances between the different components of the spectrometer can be expanded or contracted in order to adapt the acceptance of the detector to a particular kinematical region.

Other technical details can be found in the publication [AND 84].

3.2 Proposed modifications

Figure 1 shows the probable layout of the spectrometer for the proposed experiment. As has been pointed out in Section 2, we expect the thermal emission of dimuons to be enhanced in the transverse mass interval 0.6-3.0 GeV/c^2. We intend therefore to optimize the spectrometer and the trigger for low mass dimuons emitted near $y_{c.m.} = 0$. The background sources which dominate in the NA10 experiment (muon halo of the beam, and accidentals) will essentially disappear. However, multiple scattering and energy loss effects get stronger while the background induced by pion and kaon decays becomes more important as the mass of the observed pair decreases. Also, the relative background coming from pairs of pion and kaon decays scales almost linearly with the beam atomic number A_{beam}. The electromagnetic calorimeter will act as a first hadron absorber and will be followed by the NA10 absorber, which will be carbon throughout. The distance between the target centre and the absorber (i.e. the calorimeter face) will be reduced to 16 cm. The distance target-W/U plug will be increased.

The magnetic field in the toroidal magnet will be significantly reduced (B = 1.8 kG at r = 0.75 m) in order to improve considerably the acceptance in the low mass region. This does not spoil the mass resolution of the spectrometer which is dominated by multiple scattering in the absorber in the mass region below 3 GeV/c^2. The positions of the magnet, chambers and hodoscopes and the trigger will be adjusted also to favour the low mass dimuon detection.

3.3 Acceptance

Geometrical acceptance is calculated for non-thermal dimuons produced in hadronic collisions at a beam energy of 225 GeV per nucleon using the distributions given in Appendix A.

Geometrical acceptance rises rapidly with the mass from 2% at 1 GeV/c^2 to 8% at 3 GeV/c^2 as seen in Fig. 2. The final acceptance obtains as 1% at 1 GeV/c^2 and 5.5% at 3 GeV/c^2 after imposing the trigger requirements which are meant to reject the background which does not come from the target, and the selection of those events where both muons travel in the air of the magnet. Figure 3 shows that the experiment covers roughly one unit of rapidity centred at 0.5 in the centre of mass (3.5 in the laboratory).

3.4 Resolution

The dimuon mass resolution is 120 MeV around a mass of 1 GeV/c^2 and 210 MeV in the ψ region. It was calculated using simulated events and the NA10 reconstruction program. The continuum region between 1.2 and 2.7 GeV/c^2 is therefore open for study without any significant contamination from the known resonances.

The rapidity resolution is independent of y and is of the order of 0.09 at 1.0 GeV/c^2 and 0.05 at 3.0 GeV/c^2.

3.5 Background estimates

A first estimate of the background due to muons from pion and kaon decays can be derived from the present NA10 like-sign dimuon yield. This leads to an estimated dimuon contamination in p-U collisions of 3% at a mass of 1.5 GeV/c^2, the target being located 16 cm upstream from the absorber face.

This background level has been confirmed using the HIJET program [see LUD 84 and Appendix A]. Secondary pions and kaons were generated and their decay probability within the first absorption length inside the absorber was computed. The decay muons were then tracked through the apparatus using the NA10 simulation program. Each pair of accepted decay muons was taken into account with its probability. The same program was then used to generate fake muon pairs for ^{16}O-U collisions. Comparison with the ordinary (non-thermal) dimuon rate gives the background/signal ratio, shown in Fig. 4, which decreases from 35% at a mass of 1 GeV/c^2 to 25% at 2 GeV/c^2.

Finally, it is worthwhile to note that the like-sign pairs will provide an experimental estimate of the actual background.

3.6 Expected number of events

The expected number of ordinary dimuon events as given in Table 1 is calculated for a beam intensity of 10^8 particles (protons, then ^{16}O ions) every 12 s which interact with a uranium target of 1.05 cm total length (10% interaction probability for protons, 20% for ^{16}O), supposing a 20-day run with an overall efficiency of 50%. The production cross-section has been extrapolated from p-C data at 225 GeV [BRA 77] as explained in Appendix A. Thermal dimuons are not included. Figure 4 shows the mass dependence of the expected number of dimuons per burst for the ^{16}O beam.

Table 1

Expected numbers of ordinary (non-thermal) dimuons, for p-U and O-U interactions per burst, and per 20 days period.

	$M_{\mu\mu}$ (GeV/c^2)	0.5-1.2	1.2-2.7	ψ	> 4
p-U	10^8 p (= 1 burst)	6	0.4	0.7	0.04
	20 days	430,000	30,000	50,000	3,000
O-U	10^8 ions (= 1 burst)	40	4	10	0.6
	20 days	3,000,000	300,000	700,000	45,000

4. ADDITIONAL EQUIPMENT

The goals in view of which we propose to equip the target region have been outlined in Section 2: measurement of the energy density ε, distributions of charged particles and of neutral energy flow, possibly direct photon signals. The layout of the target region is shown in Fig. 5.

The high luminosity which we intend to reach poses special problems in the target region which we wish to discuss first: identification of single head-on collisions, pile-up in the detectors, radiation resistance. Next, we describe the various proposed detectors. We then discuss how the various goals are fulfilled. Finally, we outline the calibration problem.

4.1 Experimental constraints

The present NA10 spectrometer is able to accept the maximum foreseen beam intensity of 10^8 ^{16}O per two seconds provided by the SPS. The additional set-up must be able to sustain the same high intensity. Most of the new counters will provide analog signals which will be encoded in ADCs. We will construct a jitter-free dimuon trigger which will command the ADC gates by sharpening the R1-R2 hodoscope coincidence using a different layout and mean timers. Still, assuming phototube pulse durations of 10 ns and an interaction rate of $2 \times 10^7/2$ s, we find a probability of 18% that at least one extra event contributes to the ADC readings, simulating often a high transverse energy or a high charged multiplicity. We intend to flag as completely as possible such potentially misleading double interactions using the apparatus described in Section 4.4.

The target must be as thick as possible in order to give the maximum number of events. On the other hand it must be segmented in order to avoid confusion engendered either by reinteraction of spectator fragments or by the massive number of electrons created within a single compact target.

The radiation level will be enormous in and near the beam. Plastic scintillator would turn opaque in a matter of hours in the target region. In Appendix B, we evaluate the dose rates foreseen for the different detectors, and discuss the usability of quartz and of two types of scintillators. Samples of these have been heavily irradiated, and results on radiation damage are presented. We plan to use quartz Cerenkov counters near the beam focus, and plastic scintillator with a substitute for the radiosensitive POPOP everywhere else.

4.2 The electromagnetic calorimeter

Since each central O-U event produces over 200 photons, and since there is no practical way to convert and measure them separately within a distance compatible with suppressing $\pi \rightarrow \mu$ decays, we will measure only neutral energy flows, $\Delta E^{\circ}/\Delta\eta$ and $\Delta E_T^{\circ}/\Delta\eta$, i.e. the sum of the (total or transverse) energies of all photons emitted within a pseudorapidity interval $\Delta\eta$. Also, the high interaction rate compels us to use phototubes, and to choose among the few detector materials which can stand the high radiation level.

The proposed high density calorimeter is shown in Fig. 5 has a converter structure similar to the Pb fibre calorimeter which is operating successfully in the Omega spectrometer [PER 84]. It consists of a front and a tube part. The front part is made of Pb and scintillating fibres ($\phi \simeq 0.6$ mm) in a 2:1 volumic ratio ($L_{rad} = 8.3$ mm). The fibres run parallel to the beam. It has a central hole of $r_i = 1.2$ cm and an outer radius $r_e = 17$ cm. Its front face is located at 16 cm from the target centre. It covers a rapidity range $1 < \eta < 3.5$ divided into six roughly equal bins.

The transverse energy, for an element i, is $E^o_{Ti} = E^o_i \times \sin \theta_i$, where the appropriate average θ_i is determined off-line, once the primary interaction point has been determined by the active target assembly.

The tube part covers the interval $3.5 < \eta < 6.8$ and consists of five tubular elements. The first four are W/scintillator sandwiches of 1.2 and 2.5 cm inner and outer radius. In the last one, of 0.4 cm inner radius, quartz Cerenkov radiator disks which stand the expected 50 krad/h will be used instead of scintillators. All elements will be divided in six azimuthal sectors. Jets and other departures from circular symmetry can thus be recognized.

All elements will be 9-12 cm long. Depending on their angle, γ's will see between 11 and 20 L_{rad} and have 90% of their energy converted in the calorimeter. All elements will be divided into a front and a back part, the latter somewhat longer than the former. For the front calorimeter, this improves somewhat the η resolution. For the tube elements, a simple longitudinal sampling helps in subtracting the interactions of charged hadrons inside the calorimeter. The W/quartz sandwich will typically see a few photons of 10-100 GeV which leave 10% of their energy in the first 5 L_{rad}, while the numerous bremsstrahlung photons of $\lesssim 1$ GeV will deposit 30% of their energy in the same 5 L_{rad}. Longitudinal sampling will therefore increase the sensitivity for the bremsstrahlung photon effect.

The light emitted by the scintillators will be collected and transported to the phototubes by wavelength shifter bars (WLS). The PMs of the front calorimeter are located around its perimeter; those of the

tube calorimeter are located sidewise, with the light guides traversing the carbon absorber. The expected number of photoelectrons nears 50,000 per central O-U interaction, and distributes roughly evenly among the 120 elements. For the small angle W-quartz sandwich, we contemplate a quartz light guide.

Interactions of charged secondary hadrons inside the calorimeter contribute some 10-15% to the measured neutral energy, partly from the π^{o}'s created in these interactions.

4.3 The segmented active target

The active target helps to characterize, in conjunction with the calorimeter, the centrality of the nucleus-nucleus interaction. It determines the interaction point, and measures the pseudorapidity distribution of the charged particles produced, as well as the circularity of each event. The target thickness is chosen such as to give the maximum number of events compatible with the rate capability of the associated electronics, which corresponds to 20% of the nominal beam intensity of 10^{8}/2 s spill interacting in the target.

The implementation of the active target assembly is shown in Fig. 6a. A series of 20 subtargets, each 0.52 mm long, are surrounded by segmented cylindrical scintillators (three per subtarget). Each semicylinder is read by a PM so that there will be a total of about 140 PM-ADC channels. By varying the azimuthal orientation of the semicylinders we will obtain a rough azimuthal or circularity distribution. The area of the subtargets (2 x 0.5 mm^{2}) contains 90% of the beam and minimizes the contamination due to reinteractions of charged secondaries and photons.

Figure 6b displays the energy deposited in the scintillators in collisions with different impact parameters, as obtained from HIJET simulations. In all cases it is clearly possible to identify the location of the primary interaction. In cases when a spectator fragment of $A \geq 6$ reinteracts at least four subtargets further downstream, the profile of the pulse heights in the target scintillators allows the identification of reinteracting spectators. Reinteraction effects can be controlled statistically by comparing events produced in the first and last targets.

Figure 7 summarizes the results of a full simulation, selecting at random impact parameter target numbers, and target penetration before interaction. A simple criterion on the energy deposition in the first few scintillators after the struck target allows us to separate between central and peripheral events. About 67% of all events surviving such a simple cut are central. The remaining 33% have a 5-10% probability that the spectator fragment reinteracts in the target, and that the calorimeter sees an energy compatible with a central event. The resulting background is therefore small. However such a cut must be handled with care, i.e. in conjunction with the calorimeter output in order not to lose JACEE-type non-ordinary events where extreme energy densities correspond to a sudden drop in multiplicity. An EGS simulation has shown that, with the geometry chosen, the number of electrons showering into the acceptance of the active target is small compared to the number of hadrons. Consequently the cylinders can also serve to measure the pseudorapidity distribution of each event in the range $1 \leq \eta_{lab} \leq 4$.

4.4 Beam counters and interaction detector

We intend to identify the beam particle which is responsible for a trigger, using a thin (1 mm), segmented beam detector located far upstream in the beam where the beam is wide and radiation damage tolerable. It will be made of two stacks of 14 scintillators (NE 102A) symmetric with respect to the horizontal mid-plane; and must be able to recognize ^{16}O ions, ^{40}Ca ions and debris. It will be in the beam vacuum tube and its position will be adjustable by remote control. We will further build two segmented beam counters located just upstream (BEAM IN) and downstream (BEAM OUT) of the target. In view of the enormous radiation level, we use quartz in tiny pieces. The Cerenkov radiation produced by ^{16}O ions in 2 mm of quartz yields a very fast signal with 300 photoelectrons when quartz fibres bring all light to the phototube, and up to 1000 photoelectrons when a suitable wavelength shifter (WLS) technique gets hold of the UV photons. We will consider that there has probably been an interaction whenever the BEAM OUT counter produces a pulse whose height is not compatible with the mean ^{16}O signal. Each counter will be subdivided in four elements, and each element will be seen by eight discriminators of different thresholds. The timing of the outputs of each of these will be digitized for time intervals within

±10 ns from the trigger particle. The decision whether a second interaction has occurred will be made off-line on the grounds of the BEAM IN-BEAM OUT information and will forbid the use of the ADC data.

Both counters can at the same time be active targets. A pulse well above the ^{16}O level indicates a central interaction inside the counter (charged multiplicity ~ 140 >> Z^2). On the other hand, these counters can also identify ^{40}Ca ions.

4.5 Characterization of single interactions and of centrality

We wish to recapitulate here the main functions fulfilled by the target region equipment.

The beam detector allows to retain off-line those events (95%) with a single incoming particle within the time jitter of the dimuon trigger. The complete beam counter system including the BEAM-IN and BEAM-OUT counters characterizes the interactions which have taken place within ±10 ns of the event, and isolates those events (82% of 95%) whose $dN_{ch}/d\eta$ and $dE^{o}/d\eta$ data as read through some 270 ADCs are unaffected by parasite interactions.

Most non-central interactions which do not involve all 16 nucleons of the ^{16}O ion are eliminated by requiring at least 80% of the mean total neutral energy E^{o}_{tot} to be deposited in the calorimeter. Indeed, HIJET gives a natural fluctuation of ±17% on E^{o}_{tot}, and further fluctuations from early interactions of charged secondaries and from small angle losses do not add much to this. The resulting sample should contain less than 40% incomplete interactions, which will be characterized anyway by the proper $dE^{o}_{T}/d\eta$ and hence energy density ϵ, except for a less than 10% background where the fragments have reinteracted in the target and have thereby biased $dE^{o}_{T}/d\eta$ and ϵ. The pulse height in the first counters of the active target following the struck subtarget is statistically even more selective, but since the multiplicity is not necessarily a monotonously increasing function of ϵ, we prefer to perform a profile analysis of the active target with the double aim of spotting out two-step interactions and of determining the appropriate $dN_{ch}/d\eta$ for the single interactions.

Except for minor modifications in the beam identification and single interaction detection, the same procedures apply for ^{40}Ca ions, and for a primary proton beam, and also for lighter targets.

4.6 Calibration and monitoring

The totality of the detectors in the target region yield analog signals, are coupled to ADCs, and require therefore an absolute calibration. The calibration must give one number per counter, expressed in "energy deposit in MeV per ADC channel". The evolution of these numbers with time must also be monitored. Indeed, most detectors work under radiation stress and must therefore be periodically recalibrated during the runs.

The typical signals seen by individual counters range from 10 MeV to 10 GeV energy deposit per event, far beyond signals available from, for example, Co sources or U foils.

Except for the beam counters which see the signal of the unscattered ^{16}O particles, we see no possibility for self-calibration of the detectors under normal running conditions.

We intend therefore to use the ^{16}O ions of the beam for the initial calibration. For this purpose, the beam can be turned into a parallel beam of 5 cm diameter by switching off appropriate quadrupoles. The non-interacting ^{16}O ions produce then handsome narrow signals in the appropriate range for the active target as well as for all calorimeter elements. The front calorimeter must be moved horizontally and vertically until all its elements are calibrated. Each tubular element is calibrated when no other elements are located in front of it.

Once this in situ calibration has been done, monitoring is done continuously by using the mean ADC signal for each counter as obtained for a class of clean dimuon events (e.g. ψ's not preceded nor followed by parasite interactions).

The calibration strategy includes setting up and testing the complete procedure before the ^{16}O runs, in two steps.

At first, the calorimeter is exposed elsewhere to an electron beam, in order to understand its response to electrons of 1 and 10 GeV. This requires a support which turns around a point situated at 16 cm from the detector face. The gains of all PMs are equalized using protons.

Then, the complete apparatus is installed in the NA10 beam, and is calibrated and then operated with primary protons first. Thus, we intend to have a fully calibrated and working detector system at the start of the ^{16}O runs.

5. DATA ACQUISITION

The modifications proposed to the current NA10 detector imply the addition of new detection channels, which from the point of view of their integration into the data acquisition system (see Fig. 8) are of two types:

a) "Counters" which provide logical signals.

b) "Detectors" which provide analog signals.

The data provided by the "counters" will be registered by incorporating an extra crate in the RMH branch of the hodoscopes (branch 0) of the existing system. For the analog information coming from the "detectors", the addition of a tenth RMH branch will be necessary. The digitization will be achieved by 10-bit ADCs of the type LRS 2249A placed in the standard CAMAC crates, read by four ROMULUS branch drivers multiplexed to ensure that the speed with which the ADCs are read is compatible with the RMH dialogue duration, characterized by 350 ns per 16-bit word on average. (The ADC conversion time of 55 μs is not relevant here, as it takes place during the reading of the RMH branches 0-8.) The interface of the multiplexer, with ROMULUS-RMH protocol, must be constructed.

In order to record unbiased events and to take into account the increase in the number of words per event due to the additional equipment, it is necessary to increase the size of the memories of the event buffers from 2K- to 4K-words (perhaps 8K-words). For reasons of efficiency and security, it is desirable that the construction of the new memories be undertaken by the designers of the existing ones.

If, for any reasons, the availability of software and hardware maintenance support could not be guaranteed for the present four homemade microprocessors of the event buffers, they would have to be replaced by standard commercial microprocessors (e.g. CAB from LeCroy). As a consequence, the event-buffer system would have to undergo the corresponding modifications.

6. BEAM AND RUNNING TIME REQUEST

As emphasized above, we deem essential to compare proton-nucleus and nucleus-nucleus collisions at the same energy per nucleon, using the same beam quality and the same targets. In order to achieve this aim, the strategy outlined above will be followed, namely:

i) to test the calorimeter in an electron beam (probably at the PS);

ii) to set up and check the complete layout with a proton beam;

iii) to carry out the physics run in a 225 GeV proton beam; and,

iv) subsequently, with the apparatus in an optimized and reliable condition and knowing the physics to be expected in the absence of new (= collective) phenomena, to run with the ^{16}O beam, at the highest practical energy, which we will take as 225 GeV/nucleon.

A secondary proton beam of 225 GeV is excluded both for ii) and iii) mainly because of insufficient intensity ($\lesssim 10^7$ per burst) and excessive π^+ content (21%). A 450 GeV beam is adequate for ii) but not suitable for iii) since the comparison with 225 GeV/nucleon ion data would then rest on shaky ground. A front porch at 225 GeV seems to be the only viable solution for iii).

We plan to concentrate mainly on exposing a ^{238}U target, in search of new physics. A fraction not exceeding 15% of the available production beam will be used with light targets (Al or quartz, and Cu).

We request therefore:

1) About 17 days in a proton beam of $\geq 10^8$ ppp at 225 or 450 GeV, in early summer 1986, for setting up and, possibly, collecting some data.

2) About 40 days in a proton beam at 225 GeV later in 1986, in order to take proton-nucleus data a) at 10^8 protons/pulse, with the target region equipment working in order to gather about one tenth of the anticipated ion data (see Table 1 at the end of Section 3.6), and then b) at 10^9 protons/pulse, without the new apparatus, in order to accumulate at least a number of dimuons comparable with the forthcoming ^{16}O-nucleus data.

3) A ^{16}O beam with 10^8 ions per burst at 225 GeV/nucleon, for ~ 20 days or more, end 1986 or in 1987.

We will attempt to be ready to use a d beam if available. We can run eventually at ~ 50 GeV/nucleon with ^{16}O, with a considerably reduced acceptance.

We wish to express our strong interest for using a ^{40}Ca admixture in the ion beam if this should turn out to be technically feasible.

7. ORGANIZATION AND RESPONSIBILITIES

The present NA10 spectrometer, namely all the hardware, detectors, magnet and associated electronics, the Norsk Data 100/500 computer with its tape units and terminals which presently exist already, will be used in this proposed experiment. The additional equipment and technical effort is foreseen as follows.

All the new detectors, beam and interaction counters, segmented active target and electromagnetic calorimeter will be designed, manufactured and assembled in the various external laboratories of the Collaboration, with the possible exception of the converter for the calorimeter.

We plan to borrow, both from the CERN electronics pool and from the collaborating laboratories, all the CERN standard electronics namely ADCs, ECL and NIM modules, CAMAC and NIM crates, RMH modules and crates, power supplies, etc., corresponding to a total of about 280 new channels.

CERN will have the responsibility of reshaping the upstream part of the dump for the electromagnetic calorimeter location.

We will ask the Instrumentation Group of EF Division who built the present event-buffer to take care of the extension of the memories size if nothing else is changed in the system. In the case the microprocessors have to be replaced, the Collaboration will assume the responsability of the new system, with only technical advice from the EF experts. The Collaboration will also design and manufacture the ROMULUS-RMH interface mentioned in the Data Acquisition Section, with the advice and technical assistance of the specialists of RMH and ROMULUS at CERN.

The software of the on-line acquisition program will have to be adapted to the new detector configuration. The Collaboration will take charge of this work although active assistance from Norsk Data acquisition experts from the DD Division will be absolutely necessary.

Acknowledgements

We acknowledge the help of J.M. Brom, B. Escoubes, S. Escoubes-Unamuno and M. Winter, whose contributions have been essential in the genesis of this proposal, and whose collaboration will be welcomed at any time.

APPENDIX A

CHARACTERISTICS OF NUCLEUS-NUCLEUS EVENTS

A.1 Cross-sections

We assume that the inelastic cross-section is given by the low-energy result [ABD 80]:

$$\sigma(A\text{-}B) = 68.8\ (A^{1/3} + B^{1/3} - 1.32)^2 \text{ mb} .$$

In Table A.1 we give the cross-sections and interaction lengths for p-^{238}U and ^{16}O-^{238}U collisions (assuming $\sigma(p\text{-}A) = 38\ A^{0.72}$ mb).

Table A.1

Cross-sections and interaction lengths for p-U and O-U collisions

p-^{238}U		^{16}O-^{238}U	
σ (mb)	L_{int} (cm)	σ (mb)	L_{int} (cm)
1954	10.7	3764	5.5

We define central collisions as those where all the beam nucleons participate in the interaction. In a black sphere model the probability for a central collision is given by:

$$P \text{ (central collision)} = [A^{1/3} - B^{1/3})/(A^{1/3} + B^{1/3})]^2$$

For ^{16}O-^{238}U collisions this probability is 18%. HIJET gives 25% (see below, and Fig. 7).

A.2 Multiplicities and rapidity distributions

A.2.1 Monte Carlo HIJET

The distribution of secondaries produced in ^{16}O-^{238}U collisions were simulated using the HIJET simulation [LUD 84] which is based on the ISAJET pp program. The simulation assumes that nuclear reactions at very high energies can be regarded essentially as a superposition of elementary NN collisions; the leading baryon of each elementary interaction is allowed to have a subsequent NN interaction.

A.2.2 Multiplicities

In Table A.2 we compare the multiplicity of charged secondaries in $p^{238}U$ and $^{16}O-^{238}U$ at 200 GeV as given by HIJET, with experimental data [DEM 82, ELI 80], and with those given by the phenomenological analysis of [GAR 85].

Table A.2

Multiplicities of charged secondaries at an incident energy of 200 A GeV

		pp	(nucleus)	p-nucleus	$^{16}O-^{238}U$	$^{16}O-^{238}U$ (central)
DATA	[DEM 82]	7.84	(Xe)	20.7	-	-
	[ELI 80]	7.3	(Pb)	18.5	-	-
HIJET			(U)	18	190	274
MODEL	[GAR 85]	8.16	(U)	18.9	-	236.6

A.2.3 Rapidity distributions

In Fig. 9 we show the rapidity distributions in p-A (A = Xe, Pb, ^{238}U) and $^{16}O-^{238}U$ collisions at 200 GeV. Both models (HIJET and [GAR 85]) agree quite well with the existing data in p-A collisions. Extrapolations for ^{16}O-A collisions given by the two models are similar.

A.3 Dimuon cross-sections

The ordinary dimuon cross-section in $^{16}O-^{238}U$ collisions is extrapolated from p-C data [BRA 77] (Fig. 10), assuming the same A dependence as measured in p-A collisions:

$$\sigma(A\text{-}B \rightarrow \mu^+\mu^- + X) = (A \cdot B)^{\alpha}\, \sigma(pp \rightarrow \mu^+\mu^- + X)$$

with α varying from $\alpha = 0.66$ at $M = 0.5$ GeV to $\alpha = 0.85$ at $M = 2.5$ GeV. We assume $\alpha = 0.95$ for the A dependence of the ψ cross-section.

The differential distributions were taken from the p-C data, and parametrized as follows:

$$d\sigma/dx_F \sim (A - x_F)^{3.5}$$

$$d\sigma/dp_T \sim p_T \exp(-Bp_T) , \qquad B = 0.73 + 6.34/(M + 1.29) .$$

APPENDIX B

THE RADIATION ISSUE

Radiation is a crucial problem for all detectors in the target region. Table B.1 gives the radiation levels in various parts of the apparatus under the conditions of the present proposal. The charged particle emission and π^0 emission and decay have been simulated using HIJET [LUD 84], the γ showers using EGS [FOR 78].

Table B.1

Radiation doses at various detector locations

Detector	Location z *) (cm)	Location R **) (cm)	Beam area or simulation	krad/h	Mrad (10 days)
Beam counter	-1500 ca.	0	2 x 1 cm^2	26	6
Interaction detector	0	0	0.1 x 0.025 cm^2	21000	5000
Target hodoscope	0	0.4	HIJET	2.5	0.6
EM calorimeter	+20	2.3	EGS	2	0.5
	+20	1.0		21	5
	+100	1.0		30	7.5
	+180	0.4		45	11

*) z is longitudinal distance from target centre.
**) R is radial distance from beam axis.

The most critical regions are the beam focus at the target and the innermost part of the calorimeter.

The local dose rate in the beam reaches 20 Mrad/h near the target. The dose rate in the calorimeter depends essentially on the radial distance R from the beam axis, and only weakly on the longitudinal distance from the target. We contemplate the use of quartz Cerenkov counters at the target, and of a W/quartz sandwich Cerenkov calorimeter element at small angles. Quartz has been shown to be unaffected by 10^{10} rad [BEY 82].

We have studied the radiation resistance of two types of polystyrene fibres at dose rates up to 400 krad/h and total doses up to 30 Mrad. Light emission is found to decrease with total dose D as exp $(-D/D_o)$, with D_o = 20 Mrad. Light transmission is strongly affected in fibres doped with POPOP (blue spectrum peaked at 430 nm). Figure 11 gives the light output attenuated by 10 cm of fibre length, as a function of dose and dose rate, as measured two days after the end of the irradiation. Under these conditions, light output is decreased by a factor of 10 at 14 Mrad for POPOP and at 30 Mrad for K27 fibres. While we intend to pursue these studies, we conclude provisionally that polystyrene/K27 calorimeter elements located at 10 mm from the beam axis will work but will have to be carefully monitored since their light output will have decreased by 50% after 10 days at a maximum rate of 20-30 krad/h. At 23 mm from the axis, dose rates are ten times lower.

We are indebted to J.C. Thévenin for providing the scintillating fibres and to H. Schönbacher for organizing the irradiation.

REFERENCES

ABD 80 E.O. Abdrahmanov et al., Z. Phys. C 5, 1 (1980).

AND 84 L. Anderson et al., Nucl. Instrum. Methods 223, 26 (1984).

ARN 82 G. Arnison et al., CERN-EP/82-125 (1982).

BEY 82 P. Beynel et al., Compilation of radiation damage test data, Part III, Yellow Report CERN/82-10 (1982).

BIE 82 Proc. of the Bielefeld Workshop, May 1982 (eds. M. Jacob and H. Satz), (Singapore 1982).

BJO 83 J.D. Bjorken, Phys. Rev. D 27, 140 (1983).

BNL 83 Proc. of BNL Workshop, Nucl. Phys. A418 (1984).

BRA 77 J.B. Branson et al., Phys. Rev. Lett. 38, 1334 (1977).

BUR 84 T.H. Burnett et al., in HEL 84, p. 187.

CHL 84 P.V. Chliapnikov et al., Phys. Lett. 141B, 276 (1984).

DEM 82 C. De Marzo et al., Phys. Rev. D 26, 1019 (1982).

ELI 80 J.E. Elias et al., Phys. Rev. D 22, 13 (1980).

FOR 78 R.L. Ford and W.R. Nelson, EGS 3 (Electron Gamma Showers, Version 3), SLAC Report 210 (1978).

GAR 85 S. Garpman et al., Phys. Rev. D 31, 630 (1985).

GOL 85 Proposal SPSC/P 212 (March 1985).

GYU 84 M. Gyulassy, Lectures at the Academic Training Program, CERN (1984).

HEL 84 Quark matter 1984, Helsinki (ed. K. Kajantie), (Springer, 1985).

HWA 85 R.C. Hwa and K. Kajantie, Univ. Helsinki preprint HU-TFT-85-2, 1985.

ITO 81 A.S. Ito et al., Phys. Rev. D 23, 604 (1981).

KAJ 82 K. Kajantie and H.I. Miettinen, Z. Phys. C 14, 356 (1982).

LUD 84 T. Ludlam, private communication, and Proposal SPSC/P 203, Appendix A (1984).

MCL 85 L.D. McLerran and T. Toimela, Phys. Rev. D 31, 545 (1985).

OTT 83 I. Otterlund et al., Z. Phys. C 20, 281 (1983).

PER 84 D. Perrin, Contribution to the NUCLEOPHOT Symp., Strasbourg, December 1984 (to be published). See also, H. Burmeister et al., Nucl. Instrum. Methods 225, 530 (1984).

SHU 80 E.V. Shuryak, Phys. Rep. 61, 71 (1980).

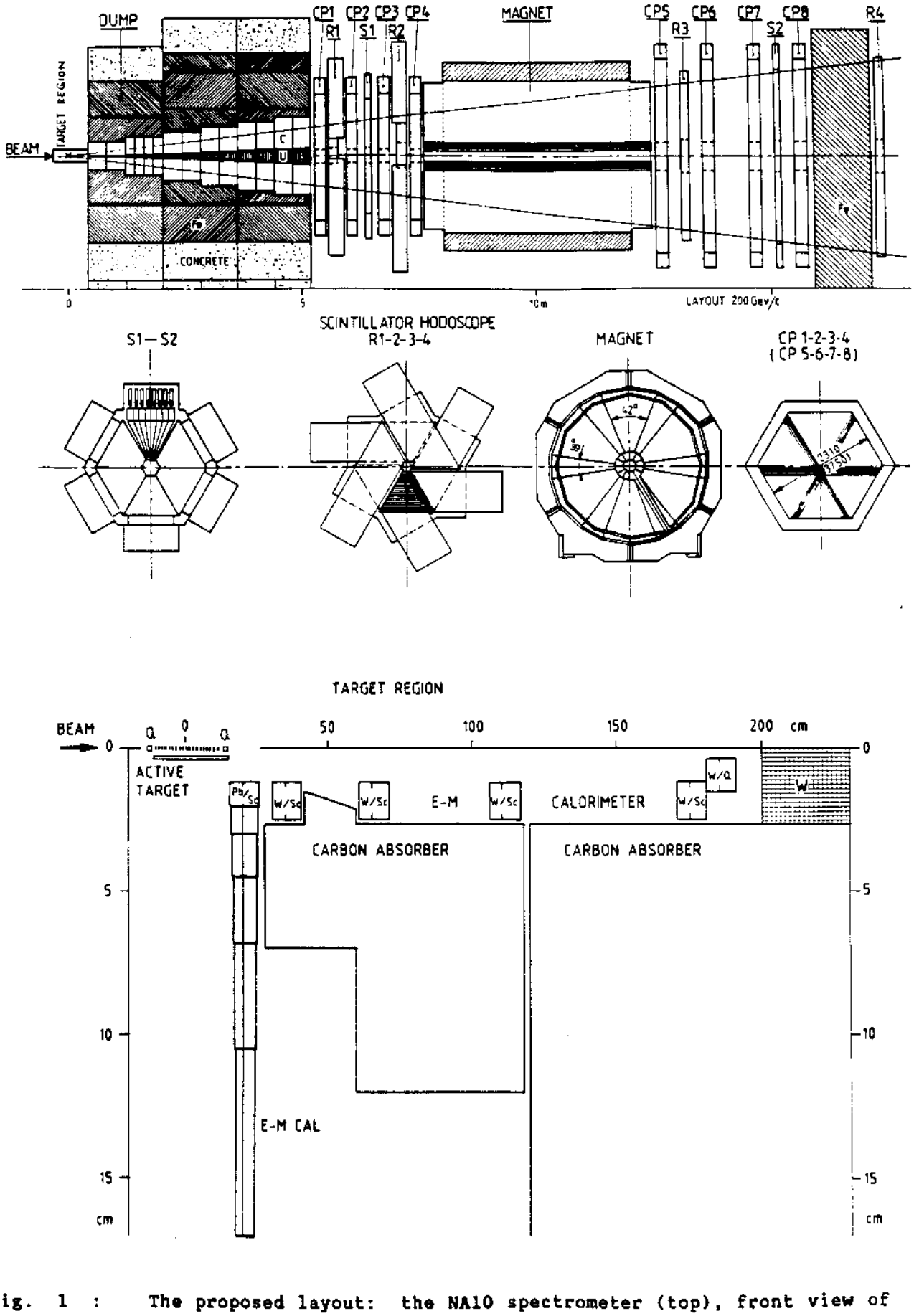

Fig. 1 : The proposed layout: the NA10 spectrometer (top), front view of its main components (middle), target region (bottom -- note scale! Q = quartz, Pb/Sc and W/Sc are sandwich structures).

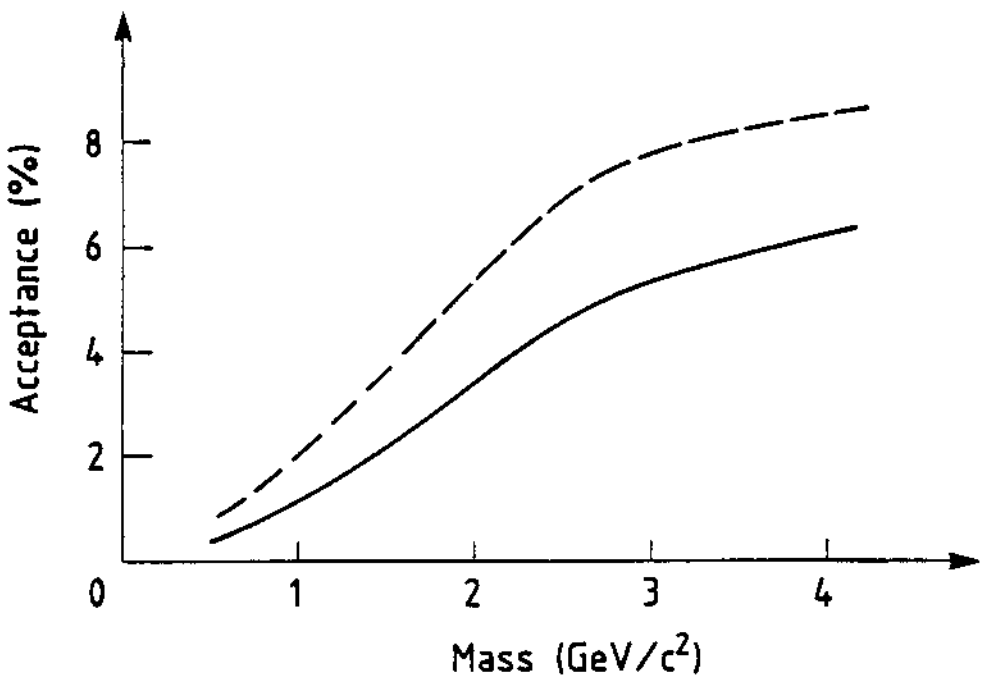

Fig. 2

Geometrical (dotted line) and final (solid line) acceptance vs. dimuon mass for ordinary dimuons.

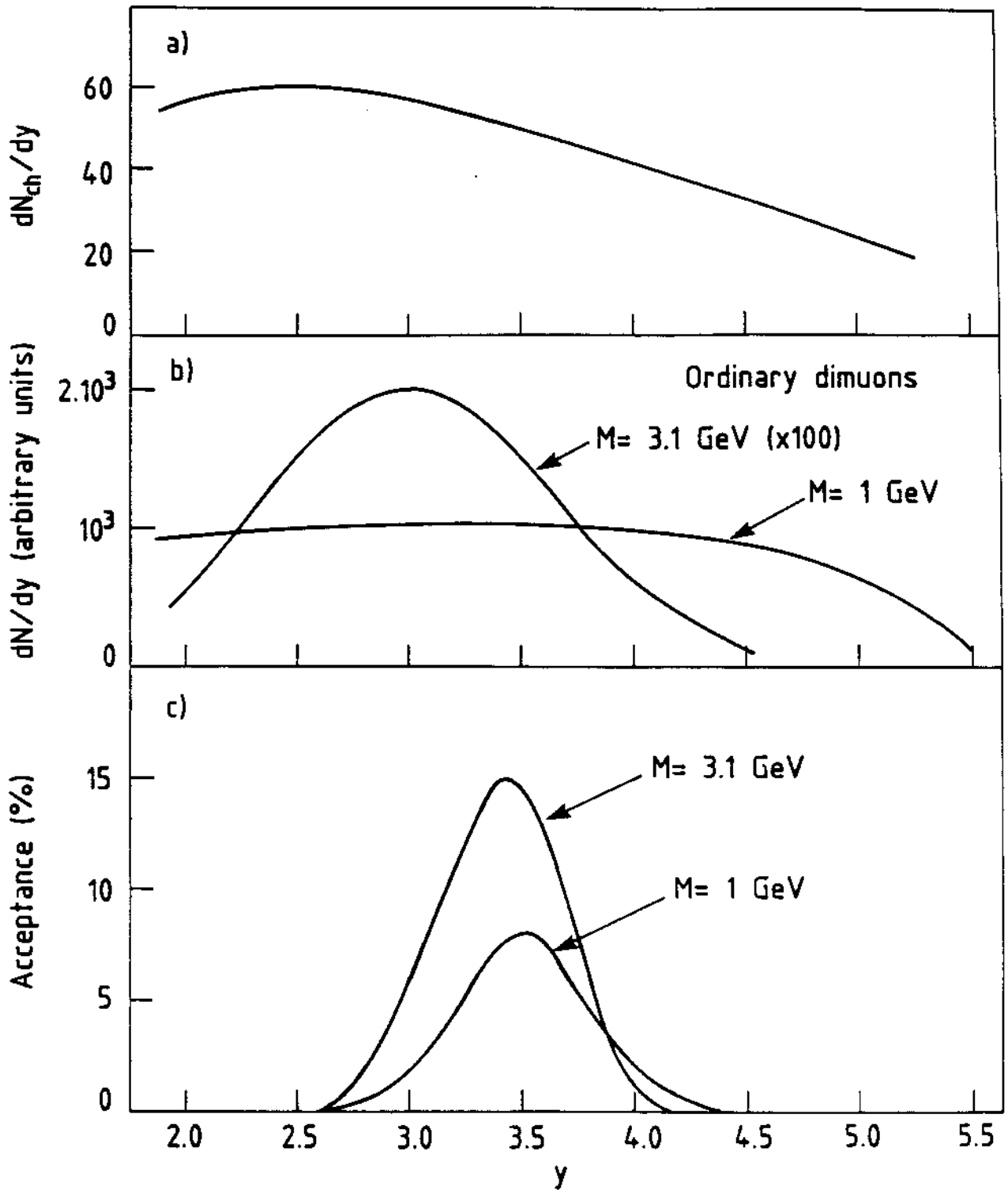

Fig. 3

Dimuon rapidity distributions. a) The charged multiplicity distribution is O-U reactions [GAR 85] is shown here to indicate that the thermal dimuons are expected to peak. b) Ordinary dimuons, from [BRA 77], peak at $y_{c.m.} = 0$ in the N-N centre of mass. c) Final acceptance of a proposed layout.

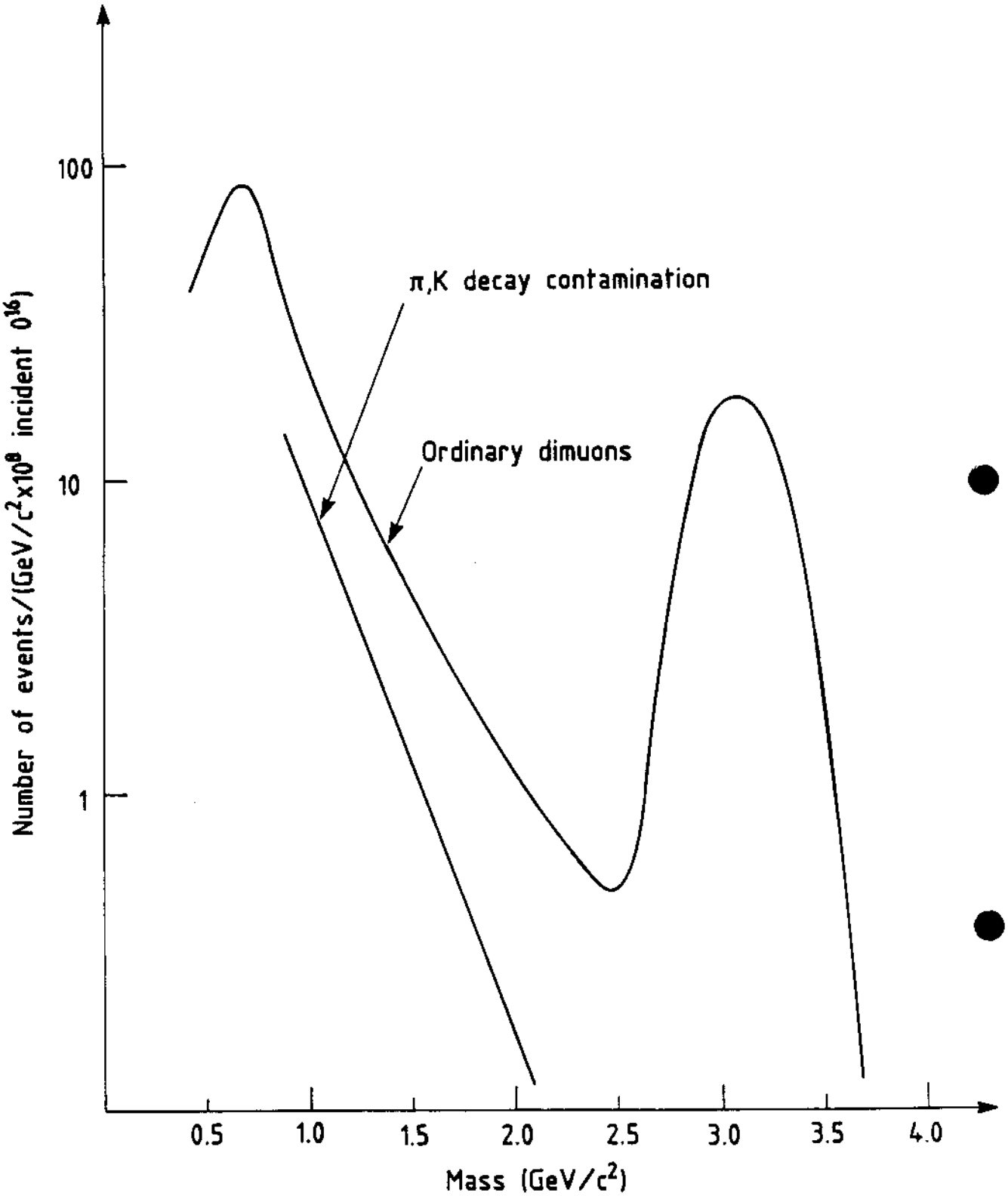

Fig. 4 : Expected event spectrum for ordinary dimuons. The expected contamination from pairs of π and K decay muons is also shown.

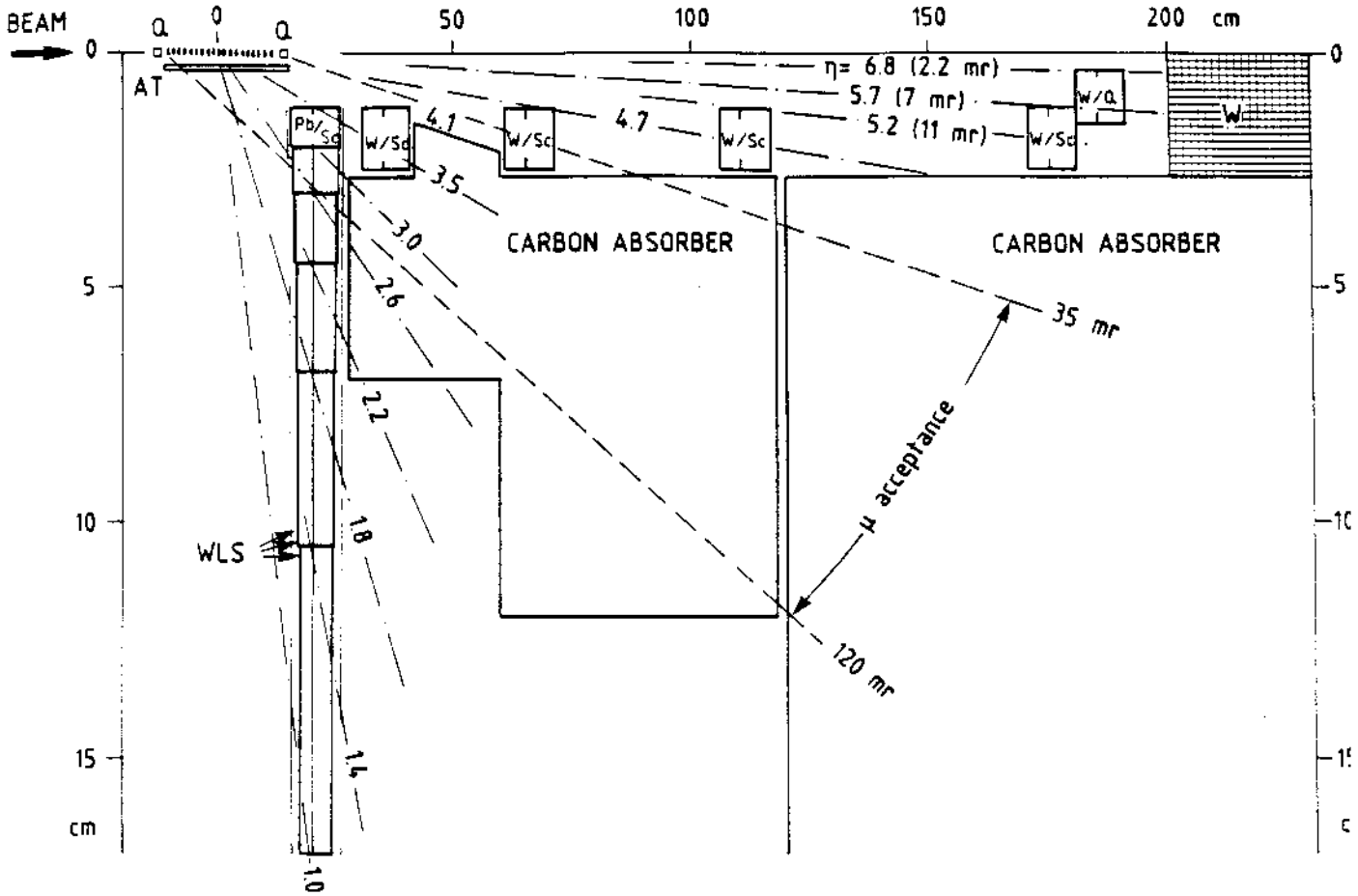

Fig. 5 : Proposed additional equipment (note distorted scale). The beam is seen by quark detectors Q and by a hodoscope located upstream (not shown). The active target AT consists of 20 subtargets surrounded by a segmented cylindrical hodoscope. The calorimeter has a front part made of Pb scintillator (Pb/Sc). Its elements are read out by wavelength shifter bars (WLS). The tube part has disconnected elements (W/Sc, W/Q) the farthest of which, a W-quartz sandwich (W/Q), will cover the angular range of the bremsstrahlung photons. Some angles and pseudorapidities are indicated. The existing hadron absorber starts at 120 cm from the target centre. Most hadrons emitted in the angular range covered by the spectrometer ("μ acceptance") find a compact absorber after an average 16 cm flight path.

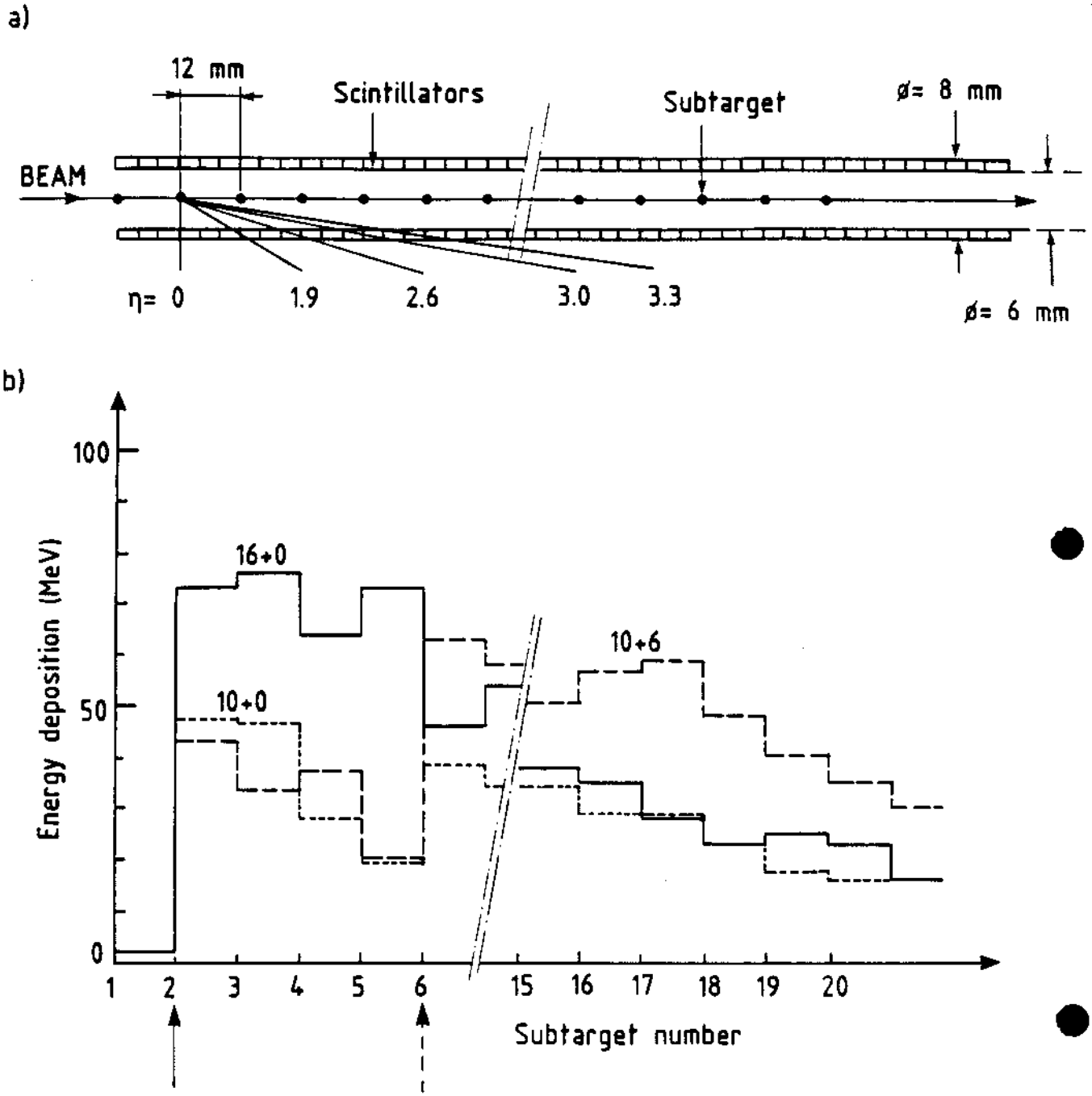

Fig. 6 : The segmented active target and characteristics of events produced in subtarget 2.

a) 20 subtargets surrounded by a segmented cylindrical hodoscope. Correspondence with the pseudorapidity scale is indicated (note inflated scale).

b) Energy deposition in grouped target hodoscope elements for individual simulated O-U events: central event (16 + 0), two peripheral events involving 10 oxygen nucleons, one without further interaction of the surviving fragments (10 + 0), one with reinteraction of the A = 6 fragment in subtarget 6 (10 + 6).

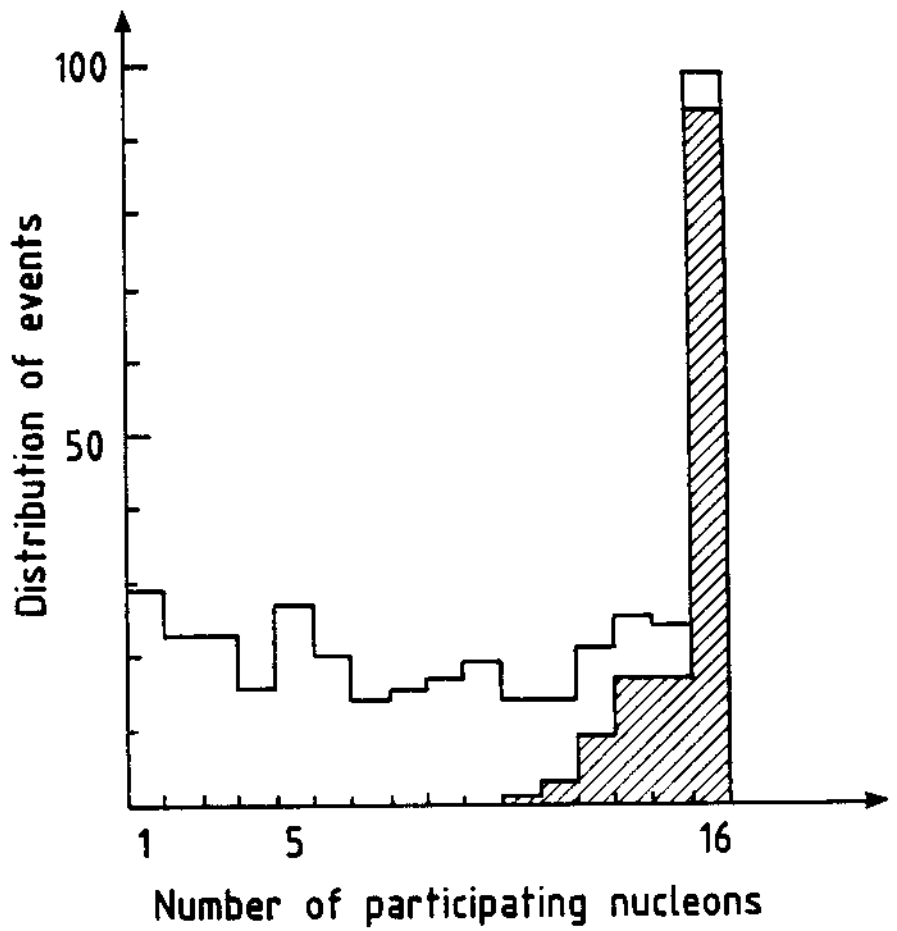

Fig. 7

Distribution of the number of participating nucleons, for 400 O-U events generated by HIJET. The hatched region corresponds to events which survive a cut in energy deposit in a selection of target hodoscope elements, and contains a majority of central events.

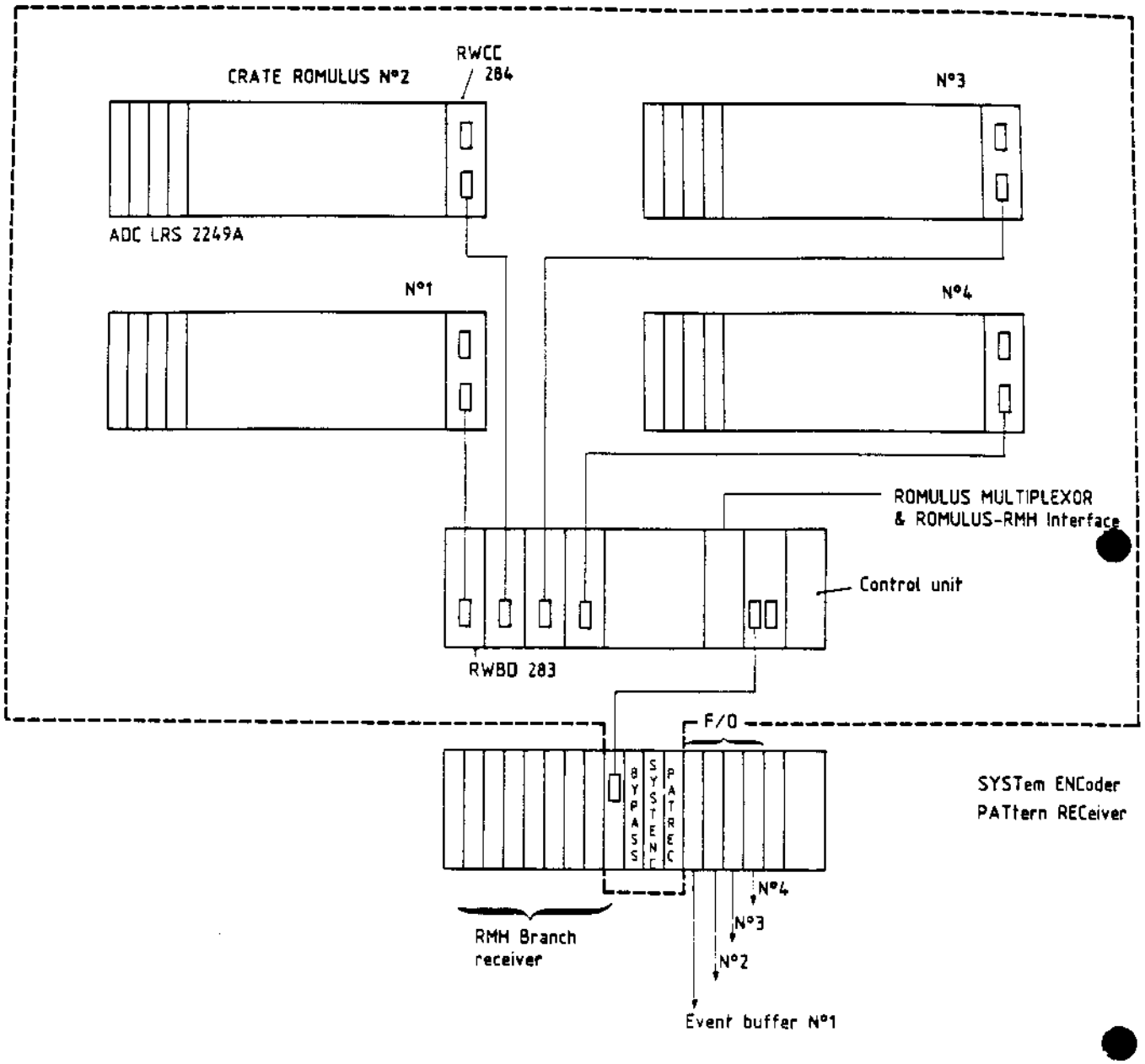

Fig. 8

The complements to the readout system needed to record the additional detectors, and their insertion into the existing system, are delimited by the dashed line. The high readout speed of the RMH system is preserved.

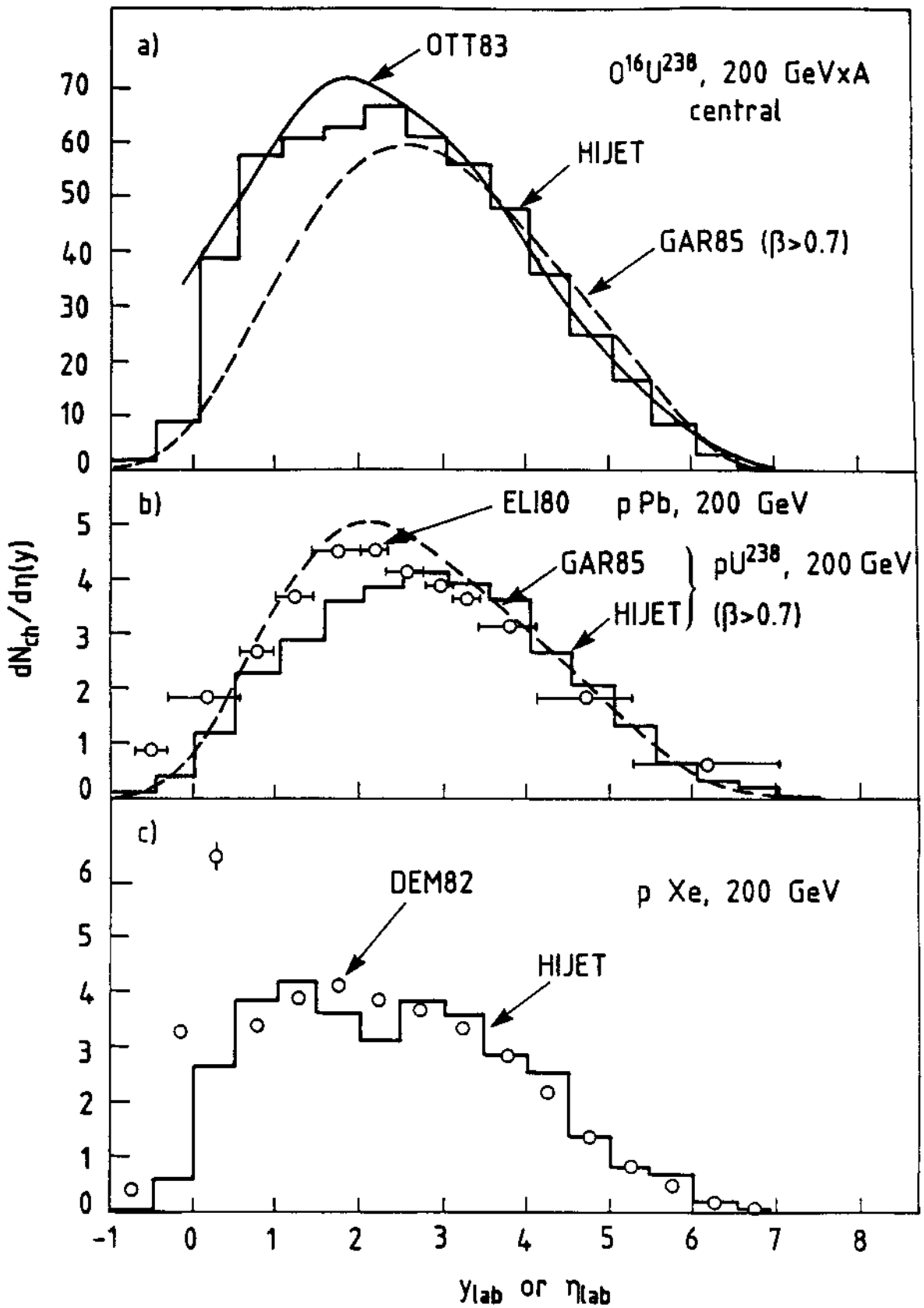

Fig. 9 : The (pseudo)rapidity distributions obtained with the HIJET simulation program are compared a) with the model of the Lund group for central O-U collisions [OTT 83, GAR 85], b) with experimental data [ELI 80) and with the model [GAR 85] for p-Pb, respectively p-U collisions, and c) with streamer chamber data [DEM 82] for p-Xe collisions.

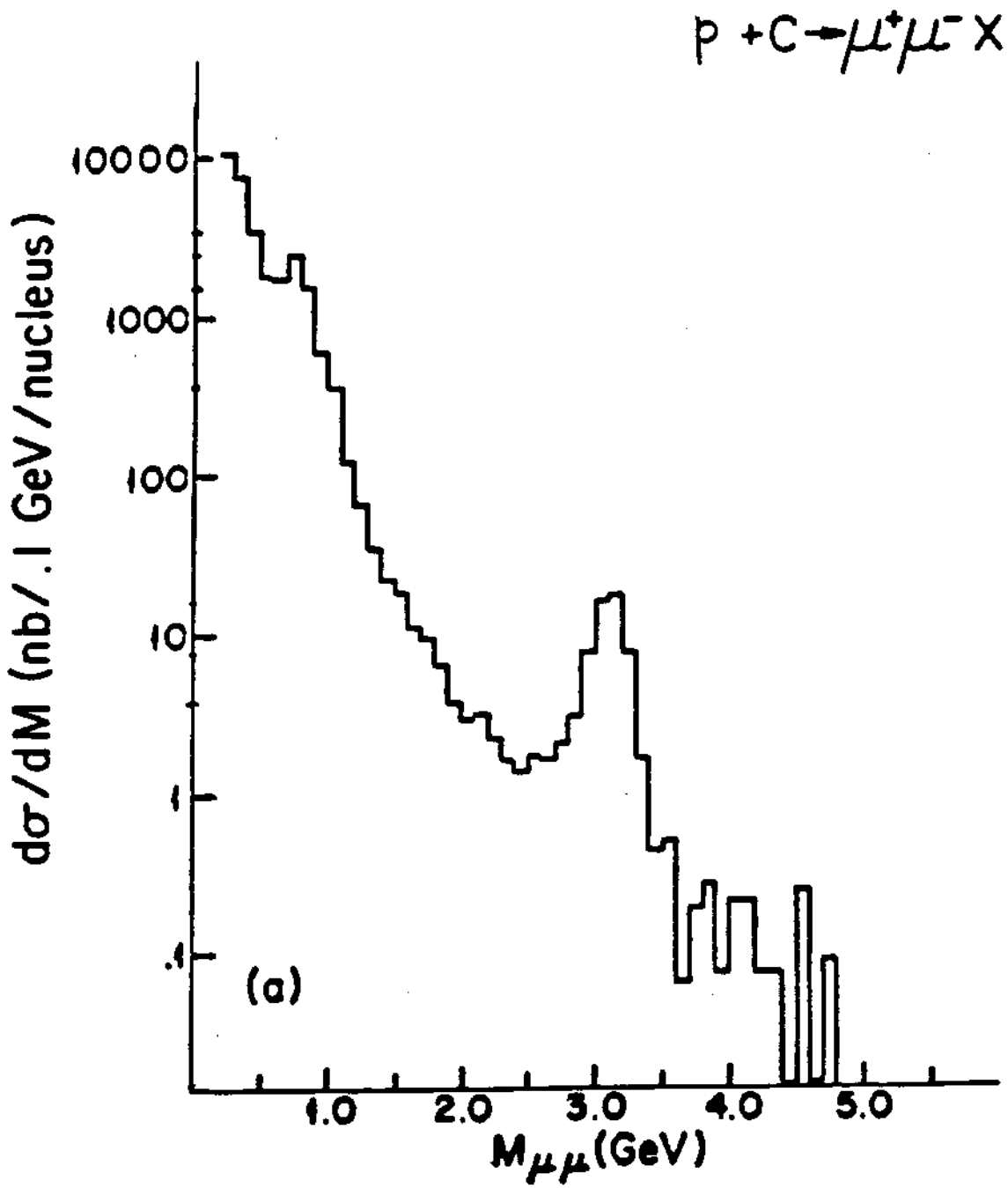

Fig. 10 : The dimuon production cross-section vs. dimuon mass obtained by [BRA 77] for pC reactions at 225 GeV. It has been used to derive the ordinary (non-thermal) dimuon spectra used in this proposal.

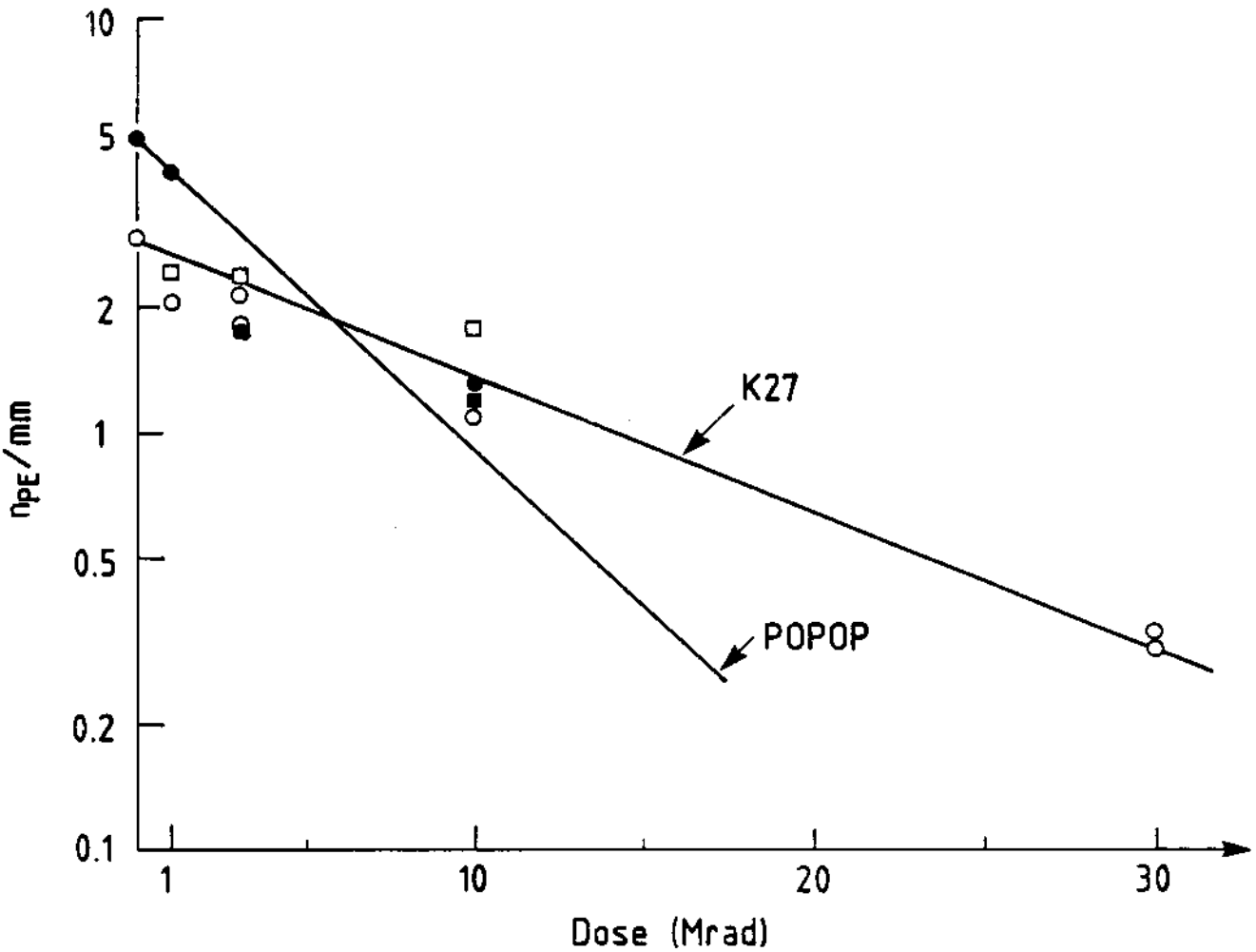

Fig. 11 : Number of photoelectrons per electron traversing 1 mm fibre at 10 cm from the fibre end, for polystyrene scintillating fibres, as measured before and two days after irradiation in a strong Cobalt source. Doses ranged from 1 to 30 Mrad and were delivered in three days (circles) or 10 days (squares). Black symbols refer to blue fibres, doped with POPOP. Open symbols are used for green fibres, doped with K27.